

Capture behavior of self-propelled particles into a hexatic ordering obstacle

Jing-Yi Li(李静怡), Jin-Lei Shi(石金蕾), Ying-Ying Wang(王英英), Jun-Xing Pan(潘俊星), and Jin-Jun Zhang(张进军)

Citation: Chin. Phys. B, 2024, 33 (**12**): 124501. DOI: 10.1088/1674-1056/ad84c6
Journal homepage: http://cpb.iphy.ac.cn; http://iopscience.iop.org/cpb

What follows is a list of articles you may be interested in

Passive particles driven by self-propelled particle: The wake effect

Kai-Xuan Zheng(郑凯选), Jing-Wen Wang(汪静文), Shi-Feng Wang(王世锋), and De-Ming Nie(聂德明)
Chin. Phys. B, 2024, 33 (**4**): 044501. DOI: 10.1088/1674-1056/ad1a8d

Rolling velocity and relative motion of particle detector in local granular flow

Ran Li(李然), Bao-Lin Liu(刘宝林), Gang Zheng(郑刚), and Hui Yang(杨晖)
Chin. Phys. B, 2022, 31 (**11**): 114501. DOI: 10.1088/1674-1056/ac7dc0

Quasi-canonicalization for linear homogeneous nonholonomic systems

Yong Wang(王勇), Jin-Chao Cui(崔金超), Ju Chen(陈菊), Yong-Xin Guo(郭永新)
Chin. Phys. B, 2020, 29 (**6**): 064501. DOI: 10.1088/1674-1056/ab8627

Biomechanical behaviors of dragonfly wing: relationship between configuration and deformation

Ren Huai-Hui(任淮辉), Wang Xi-Shu(王习术), Chen Ying-Long(陈应龙), and Li Xu-Dong(李旭东)
Chin. Phys. B, 2012, 21 (**3**): 034501. DOI: 10.1088/1674-1056/21/3/034501

Capture behavior of self-propelled particles into a hexatic ordering obstacle

Jing-Yi Li(李静怡), Jin-Lei Shi(石金蕾), Ying-Ying Wang(王英英), Jun-Xing Pan(潘俊星)[†], and Jin-Jun Zhang(张进军)[‡]

School of Physics and Information Engineering, Shanxi Normal University, Taiyuan 030032, *China*

(Received 15 July 2024; revised manuscript received 10 September 2024; accepted manuscript online 9 October 2024)

Computer simulations are utilized to investigate the dynamic behavior of self-propelled particles (SPPs) within a complex obstacle environment. The findings reveal that SPPs exhibit three distinct aggregation states within the obstacle, each contingent on specific conditions. A phase diagram outlining the aggregation states concerning self-propulsion conditions is presented. The results illustrate a transition of SPPs from a dispersion state to a transition state as persistence time increases within the obstacle. Conversely, as the driving strength increases, self-propelled particles shift towards a cluster state. A systematic exploration of the interplay between driving strength, persistence time, and matching degree on the dynamic behavior of self-propelled particles is conducted. Furthermore, an analysis is performed on the spatial distribution of SPPs along the *y*-axis, capture rate, maximum capture probability, and mean-square displacement. The insights gained from this research make valuable contributions to understanding the capture and collection of active particles.

Keywords: self-propelled particles, complex obstacle, capture behavior

PACS: 45.50.–j, 05.40.–a, 02.50.–r, 05.40.Jc **DOI:** 10.1088/1674-1056/ad84c6

1. Introduction

Active matter, originating from biological systems, is prevalent in nature and refers to substances that can actively absorb energy from the external environment and move spontaneously. This phenomenon is exemplified by the migration behavior of fish shoals on a macro scale and the movement of microscopic cells.[1–8] The collective behavior exhibited by active substances demonstrates rich non-equilibrium characteristics,[9] including motility-induced phase separation,[10–13] hexatic ordering,[14–16] and clustering.[17–19] As a result, active matter holds significant potential for applications not only in life sciences but also in the development of micro-devices and drug transport systems. However, it is noteworthy that active matter often operates in complex environments rather than uniform ones, as seen in the spread and invasion of cancer cells within the body[20–23] and the movement of molecular motor micro-machines shuttling proteins between cells.[24,25] Consequently, the study of active matter's movement behavior in complex obstacle environments has garnered substantial attention from both physical and biological researchers.[26–36]

In recent decades, researchers have made significant advances in developing new models and computational techniques aimed at understanding the unique multi-particle effects and aggregation phenomena exhibited by active matters in complex obstacle environments.[37–42] Bhadra Hrishikesh and Ethayaraja Mani identified a capture effect of active particles on passive particles, resulting in the formation of large clusters and phase separation within mixed systems of active and passive particles.[43] Conversely, Ma *et al.* observed the formation of large clusters by active particles under specific conditions.[44] Furthermore, Pan *et al.* demonstrated that active particles have the ability to gather and rotate around obstacles in a bath containing large obstacles.[45] Additionally, Shi *et al.* showed that active objects can navigate through complex media.[27] These findings have generated curiosity surrounding the capture behavior of self-propelled particles in intricate obstacle environments, prompting questions about leveraging obstacles to capture dispersed active particles, elucidating the physical mechanisms underlying capture behavior, and optimizing the capture efficiency. Thus, our study investigates the capture of active particles featuring a repulsive Weeks–Chandler–Anderson (WCA) potential in complex obstacle scenarios, focusing on the impact of driven strength, persistence time, and obstacle spacing ratio on the dynamic behavior and capture probability of self-propelled particles through Brownian dynamics simulation.

2. Model and methods

We examine a two-dimensional model system illustrated in Fig. 1. The obstacle arrays are made up of round particles that share the same size as the self-propelled particles (SPPs). The obstacle is fixed in the middle of the simulation box, forming a hexagonal lattice configuration. To create a dense porous medium, we establish a lattice constant of $a = 1.938\sigma$ for the array. Before initiating the simulation, round SPPs with mass m and size σ are randomly distributed, along with their initial propelling directions being arbitrarily assigned. Throughout

[†]Corresponding author. E-mail: panjx@sxnu.edu.cn
[‡]Corresponding author. E-mail: zhangjinjun@sxnu.edu.cn

© 2024 Chinese Physical Society and IOP Publishing Ltd

the simulation, all particles interact via the purely repulsive WCA potential[46]

$$U_{\mathrm{WCA}}(r)=\begin{cases}4\varepsilon\left[\left(\frac{\sigma}{r}\right)^{12}-\left(\frac{\sigma}{r}\right)^{6}\right]+\varepsilon, & r<r_{\mathrm{c}},\\ 0, & r>r_{\mathrm{c}},\end{cases} \tag{1}$$

with a cutoff at $r_{\mathrm{c}}=2^{1/6}\sigma$. The motion of SPPs is described by the Langevin equations

$$m\ddot{\boldsymbol{r}}_i=-\nabla_i U_i-\zeta\dot{\boldsymbol{r}}_i+\boldsymbol{F}_{\mathrm{a}}\hat{\boldsymbol{\mu}}_i(t)+\sqrt{2\zeta k_{\mathrm{B}}T}\boldsymbol{\eta}_i(t), \tag{2}$$

$$\dot{\theta}_i=\sqrt{2D_{\mathrm{r}}}\xi_i(t). \tag{3}$$

Equation (2) describes the translational motion of SPPs and equation (3) depicts the coupled rotational kinetics of the propelling direction. $\boldsymbol{r}_i$ is the position vector of the ith SPP and U_i is its total interaction energy. We set the translational friction coefficient $\zeta=10$, which is large enough so that the motion of SPPs is effectively overdamped. The propelling forces on the SPPs have the same strength F_{a} but independent propelling directions. For example, the direction of the ith SPP $\hat{\boldsymbol{\mu}}_i=(\cos\theta_i,\sin\theta_i)$ rotates independently and diffusively with the rate D_{r}. The inverse of the rotational diffusion rate $(1/D_{\mathrm{r}})$ characterizes the persistence time of the self-propelled motion. $\boldsymbol{\eta}_i(t)$ and $\xi_i(t)$ are unit-variance Gaussian white noises. We choose m, σ and ε as scaling units (hence time unit $\tau=\sqrt{m\sigma^2/\varepsilon}$) and set the scaled temperature $k_{\mathrm{B}}T=1$. We keep the inertial terms in Eq. (2) so that the velocity–Verlet algorithm (by the home-modified software LAMMPS) and a large time step could be used.[47,48] The simulation box size is $200\sigma\times100\sigma$. The periodic boundary condition is adopted. Typically, the simulation times are $10^7\tau$ time steps. Unless otherwise specified, the global average concentration of SPPs ϕ is 20%.

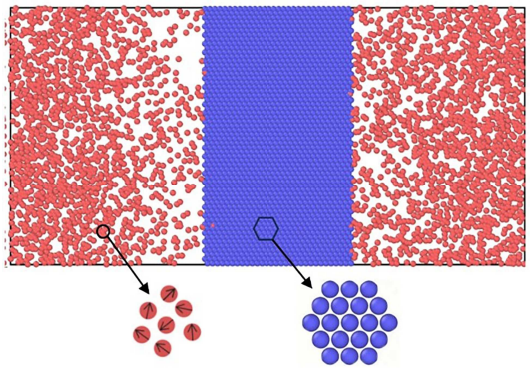


Fig. 1. Model diagram of self-propelled particles system in obstacle.

3. Result and discussion

First, we analyze the capture behavior of SPPs under various self-propelled conditions. In the absence of obstacles, the SPPs are uniformly distributed throughout the system (see the inset in Fig. 2(a)). When an obstacle is set into the system, three distinct representative aggregation patterns occur in the system (as shown in Fig. 2(a)). These patterns are associated with the dispersion state (Fig. 2(a1)), transition state (Fig. 2(a2)), and cluster state (Fig. 2(a3)). The distribution of SPPs along the y-axis in obstacles is depicted in Fig. 2(b), denoted as N_{a}, which represents the number of particles. In the case of cluster state, SPPs aggregate in obstacle in the vertical direction and form one large cluster. The particle density distribution exhibits distinct characteristics, with a pronounced peak observed on the N_{a}–y curve (the blue line in Fig. 2(b)). The microstructure of these clusters displays a large-scale hexagonal ordering. Conversely, in the cases of dispersion state and transition state, the particle density distribution lacks clear features without pronounced peak, and SPPs are uniformly spread throughout the obstacle area. Further observation indicates that at small driven strength and long persistence time, SPPs form multiple localized cluster structures within the obstacle. In the transition state, the microstructure of these clusters exhibits a short-range hexagonal ordering and these ordering structures are not observed in the dispersion state.

We conduct extensive simulations to examine the capturing processes under varying levels of driven strength (F_{a}) and persistence time ($1/D_{\mathrm{r}}$). The outcomes of these simulations are presented in Fig. 2(c). When the driven strength is small ($F_{\mathrm{a}}\leq25$) and the persistence time is short ($D_{\mathrm{r}}\geq0.04$), SPPs exhibit low persistence and slow movement. The particles have relatively short directional durations and frequent collisions, which enable them to "freely" navigate through obstacles without forming clusters. Consequently, the SPPs display a dispersed state. As the persistence time decreases to $D_{\mathrm{r}}\leq0.03$ while F_{a} remains in the range of 5 to 20, the persistence time of SPPs increases, leading to a reduction in particle collisions. This, in turn, raises the likelihood of particles entering obstacles and forming small clusters within specific areas. These small clusters further impede the migration of internal particles. Ultimate, SPPs gather into clusters of different sizes in the obstacle; and the clusters are dispersed throughout the obstacle, resulting in transition states. On the other hand, for F_{a} values exceeding 25, SPPs quickly enter obstacles and form dense clusters, hindering the migration of internal particles and leading to the formation of a large cluster.

To assess the capture process quantitatively, we statistically calculate the probability of SPPs being captured by the obstacle, denoted as $P=(N_{\mathrm{b}}/N_{\mathrm{a}})\times100\%$, where N_{b} represents the total number of SPPs captured by the obstacle, and N_{a} is the total number of SPPs in the system. The evolution of the capture probability of the obstacle to SPPs over time at different driven force (F_{a}) of 5, 10, and 30 is illustrated in Figs. 3(a)–3(c). The time for the obstacle to reach the steady capture is denoted by t_{sc}.

In the case of $F_{\mathrm{a}}=5$, the time t_{sc} increases with the rise in

D_r, as shown in Fig. 3(a). Upon increasing F_a to 10, the time t_{sc} decreases, and with a further increase in D_r, the time t_{sc} also rises, as depicted in Fig. 3(b). For F_a greater than or equal to 30, steady capture can be achieved within $t \leq 2000\tau$, and the capture time is minimally affected by D_r, as demonstrated in Fig. 3(c). In general, t_{sc} decreases progressively with an increase in F_a and a decrease in D_r. Additionally, we determine the maximum capture probability (P_{max}) under various propulsion conditions (Fig. 3(d)). First, when $F_a \geq 10$, the maximum capture probability (P_{max}) increases with the decrease of D_r, and P_{max} is close to 100% at $D_r = 0.001$. Second, for $F_a \geq 5$, P_{max} also increases with the decrease of D_r, and it is worth noting that there is an anomaly at $D_r = 0.001$, indicating that SPPs are more likely to escape from obstacles under this specific condition. Third, P_{max} increases with the increase of F_a at the same D_r.

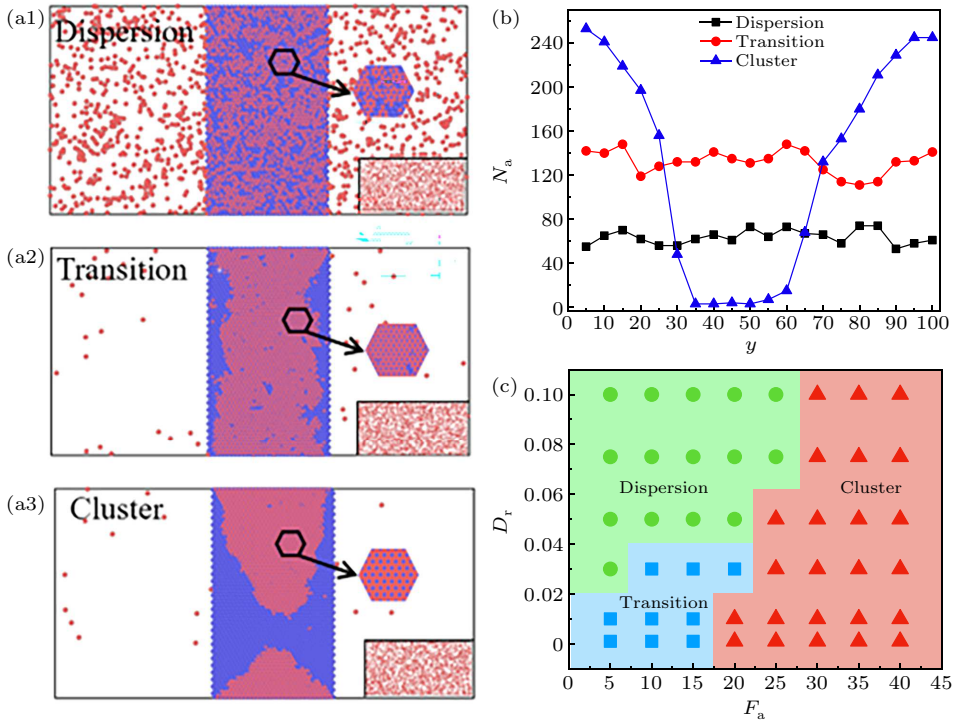


Fig. 2. (a) Representative aggregation patterns of the system for (a1) $F_a = 10$, $D_r = 0.001$, (a2) $F_a = 10$, $D_r = 0.1$, (a3) $F_a = 30$, $D_r = 0.001$; the inset figures show the morphology under the corresponding parameters when there is no obstacle. The red points represent SPPs; the blue points mimic a hexagonal array of obstacles. (b) The variation of the number of SPPs N_a in the obstacle along the y-axis under different states. (c) Phase diagram in F_a–D_r space of the states of SPPs.

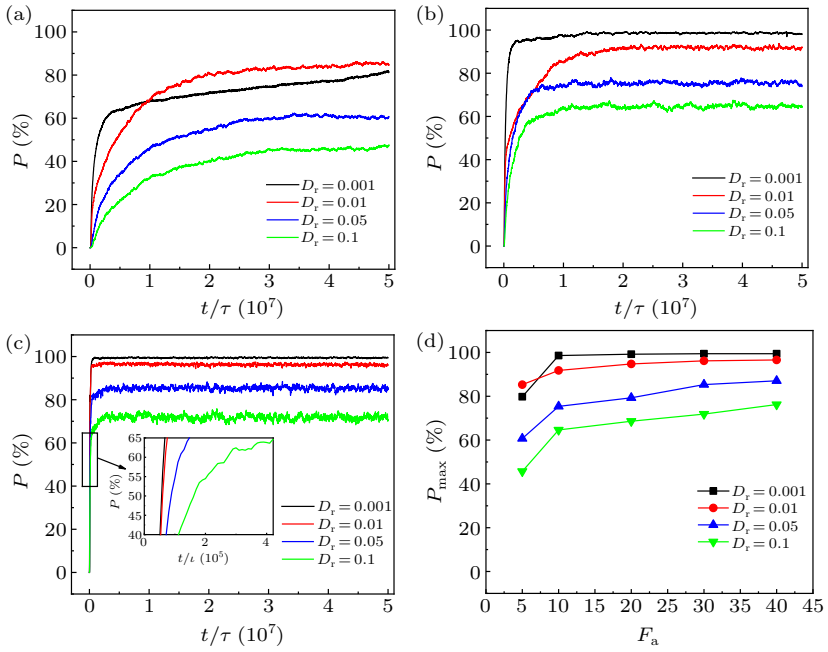


Fig. 3. (a)–(c) The evolution of the capture probability of the obstacle to SPPs over time at different driven force (F_a) of 5, 10, and 30. (d) The maximum capture probability (P_{max}) under various propulsion conditions.

In order to understand the dynamic mechanism of the above phenomena, we calculate the ensemble average of the mean-square displacement (MSD) as a function of the time lag time Δt. MSD is calculated as follows:[49,50]

$$\mathrm{MSD} = \frac{1}{N}\sum_{i=1}^{N}\frac{1}{T_{\max}-\Delta t}\int_{0}^{T_{\max}-\Delta t}[\boldsymbol{r}(t+\Delta t)-\boldsymbol{r}(t)]^2\,\mathrm{d}t, \quad (4)$$

where $T_{\max}$ is the total simulation run time, $\boldsymbol{r}(t)$ represents the position of the tracer at an initial time t, $\boldsymbol{r}(t+\Delta t)$ denotes the tracer position after the lag time Δt, and N is the total number of independent trajectories. The time exponent $\alpha(t)$ is defined as

$$\alpha(t) = \frac{\mathrm{d}\log(\mathrm{MSD})}{\mathrm{d}\log(t)}. \quad (5)$$

The plots of MSD against t on the log–log scale and the corresponding time exponents (t) on log–linear scale are shown in Fig. 4. In the early times, SPPs exhibit a super-diffusive behavior where the growth rate of MSD is high ($1 < \alpha(t) < 2$). In scenarios with long persistence times ($D_{\mathrm{r}} = 0.001$) and low driven strength ($F_{\mathrm{a}} = 5$) (refer to the black line in Fig. 4), SPPs consistently display super-diffusive characteristics throughout their movement. However, upon encountering obstacles, the SPPs' movement is impeded, causing a slowdown in the growth rate of MSD, leading to particles aggregation within the obstacle and resulting in a transition state (refer to Fig. 2(a2)). By $t = 1\times10^7\tau$, the aggregation state inside the obstacle stabilizes, and the rate of change in MSD decreases to its minimum. Meanwhile, SPPs that are unable to penetrate the obstacle obtain a higher growth rate of MSD, compensating for the loss of MSD exhibited by SPPs within the obstacle, and the exponent $\alpha(t)$ slightly increases (refer to Movie S1). Conversely, when $F_{\mathrm{a}} = 5$ and $D_{\mathrm{r}} = 0.1$ (refer to the red line in Fig. 4), SPPs that manage to enter the central region of the obstacle become effectively "pinned" within, inducing a swift transition of the system to a sub-diffusive state ($\alpha(t) < 1$). This pinning of SPPs impedes the entry of additional particles, culminating in the system forming a dispersed state (refer to Fig. 2(a1)). In cases of $F_{\mathrm{a}} = 30$ and $D_{\mathrm{r}} = 0.001$ (refer to the green line in Fig. 4), nearly all SPPs swiftly infiltrate the obstacle, leading to a rapid decrease in α. Following the entry of SPPs into the obstacle, there ensues a period of structural reorganization within the cluster, evolving from a dispersed state into complete hexagonal ordering (refer to Fig. 2(a3)). Throughout this transition, the change in α approaches zero, and SPPs exhibit normal diffusive behavior at $\alpha(t) = 1$. Subsequently, except for a few particles positioned outside the obstacle and at the cluster's periphery, the MSD of SPPs dwindles close to zero, signifying a shift in the dynamics of SPPs towards sub-diffusive behavior (refer to Movie S2). For $F_{\mathrm{a}} = 30$ and $D_{\mathrm{r}} = 0.1$ (refer to the blue line in Fig. 4), the MSD continues to decrease until $t = 1\times10^7\tau$. Subsequently, the system reaches a dynamic equilibrium, with α stabilizing as a constant.

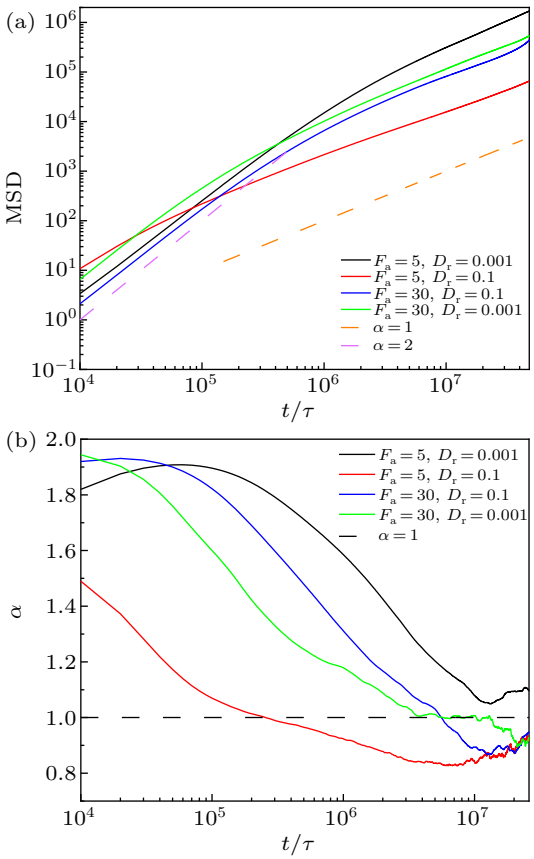


Fig. 4. At $F_{\mathrm{a}} = 5$, $D_{\mathrm{r}} = 0.001$; $F_{\mathrm{a}} = 5$, $D_{\mathrm{r}} = 0.1$; $F_{\mathrm{a}} = 30$, $D_{\mathrm{r}} = 0.1$ and $F_{\mathrm{a}} = 30$, $D_{\mathrm{r}} = 0.001$. (a) Log–log plot of MSD vs. t of the SPPs. (b) Log–linear plot of $\alpha(t)$ vs. t of the SPPs.

Furthermore, we consider the effect of obstacle on the capture behavior. We define the matching degree as $R = (a-d_1)/d_2$, where a is the distance between the centers of two adjacent obstacle particles, d_1 is the diameter of the obstacle particle and d_2 is the diameter of the self-propelled particle.

The maximum capture probability ($P_{\max}$) as a function of R is statistically calculated under different matrix structures in the case of $F_{\mathrm{a}} = 30$ and $D_{\mathrm{r}} = 0.001$, as shown in Fig. 5. When the obstacle particles are arranged in a hexagonal structure. The maximum capture probability follows a non-monotonous trend with the increase in the matching degree. When $R < 0.9$ (indicating obstacle particles spacing $(a-d_1)$ smaller than the particle diameter d_2), the SPPs tend to cluster at the edge of the obstacle, and it is difficult to enter the obstacle. As R ranges from 0.9 to 1.0 (indicating obstacle particles spacing $(a-d_1)$ equivalent to the particle diameter d_2), SPPs tend to aggregate within the obstacle, forming a stable cluster state with a maximum capture probability $P_{\max}$ nearing 100%. Subsequently, as R further increases, the migration of SPPs in obstacles becomes easier, which also means that it is easier for SPPs to escape from the obstacle, resulting in a decrease in $P_{\max}$. When $R \geq 1.7$, the obstacle particles spacing is large enough to make

the SPPs through freely, consequently resulting in a substantial decrease in P_{max}. In addition, when the obstacles are arranged in a square structure, the trend of the maximum capture probability changing with the matching degree is similar to that of hexagonal obstacles. However, square obstacles exhibit a lower P_{max} and a narrower range of matching degrees that can achieve higher capture probabilities. This is because square obstacles create channels that facilitate easier traversal for SPPs. Meanwhile, we also consider random structure obstacles and find that due to the scattered distribution of obstacle particles, SPPs are unable to form a dense stacking structure in the obstacles.

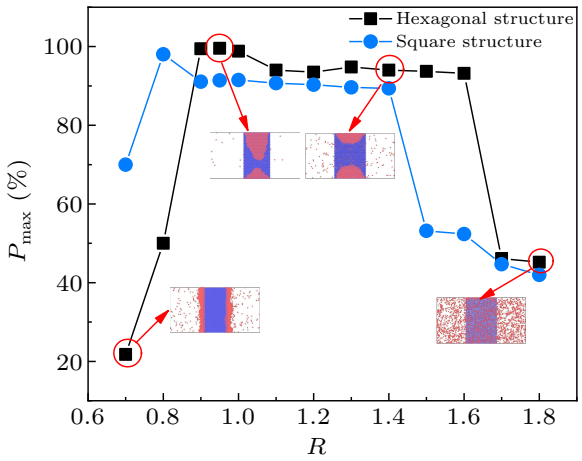


Fig. 5. The maximum capture probability (P_{max}) as a function of R under different matrix structures ($F_a = 30$, $D_r = 0.001$).

4. Conclusion

In this paper, the capture behavior of self-propelled particles in a hexatic ordering obstacle is investigated by using molecular dynamics. The study reveals the following key findings. (i) Self-propelled particles exhibit three distinct states, dispersion state, transition state, and cluster state, depending on the prevailing self-propelled conditions. (ii) The optimal capture state and maximum capture probability (P_{max}) closed to 100% can be obtained with the condition of large F_a and small D_r. (iii) SPPs demonstrate varied dynamic behaviors across different aggregation states, transitioning from super-diffusion to sub-diffusion behavior upon encountering obstacles. (iv) The capture efficiency is significantly influenced by the matching degree between the spacing of obstacle and the SPPs. A higher capture probability is observed within the range of $0.9 < R < 1.0$. It is worth mentioning that this study exclusively considers SPPs governed by idealized WCA potential, and our results provide the theory and model reference for further research. Subsequent studies can introduce more complex interaction potentials to make it closer to the real system.

Acknowledgment

Project supported by the Natural Science Foundation of Shanxi Province, China (Grant Nos. 202303021212148 and 202103021223245).

References

[1] Makris N C, Ratilal P, Jagannathan S, Gong Z, Andrews M, Bertsatos I, Godø O R, Nero R W and Jech J M 2009 *Science* **323** 1734
[2] Becco Ch, Vandewalle N, Delcourt J and Poncin P 2006 *Phys. Stat. Mech. Its Appl.* **367** 487
[3] Sarkar D, Gompper G and Elgeti J 2021 *Commun Phys.* **4** 36
[4] Paxton W F, Kistler K C, Olmeda C C, Sen A, St. Angelo S K, Cao Y, Mallouk T E, Lammert P E and Crespi V H 2004 *J. Am. Chem. Soc.* **126** 13424
[5] Bechinger C, Di Leonardo R, Löwen H, Reichhardt C, Volpe G and Volpe G 2016 *Rev. Mod. Phys.* **88** 045006
[6] Surrey T, Nédélec F, Leibler S and Karsenti E 2001 *Science* **292** 1167
[7] Ramaswamy S 2010 *Ann. Rev. Condensed Matter Phys.* **1** 323
[8] Reynolds C W 1987 *SIGGRAPH Comput. Graph* **21** 25
[9] Schweitzer F 2003 *Brownian Agents and Active Particles: Collective Dynamics in the Natural and Social Sciences* (Berlin: Springer-Verlag) pp. 51–131
[10] Tailleur J and Cates M E 2008 *Phys. Rev. Lett.* **100** 218103
[11] Cates M E and Tailleur J 2015 *Annu. Rev. Condens. Matter Phys.* **6** 219
[12] Fily Y and Cristina Marchetti M 2012 *Phys. Rev. Lett.* **108** 235702
[13] Stenhammar J, Tiribocchi A, Allen R J, Marenduzzo D and Cates M E 2013 *Phys. Rev. Lett.* **111** 145702
[14] Redner G S, Hagan M F and Baskaran A 2013 *Phys. Rev. Lett.* **110** 055701
[15] Digregorio P, Levis D, Suma A, Cugliandolo L F, Gonnella G and Pagonabarraga I 2018 *Phys. Rev. Lett.* **121** 098003
[16] Tang Y W, Chen S Y, Bowick M J and Bi D 2024 *Phys. Rev. Lett.* **132** 218402
[17] Peruani F, Deutsch A and Bär M 2006 *Phys. Rev. E* **74** 030904
[18] Pilla R T and Mani E 2022 *J. Phys. Condens. Matter* **34** 245101
[19] Son K, Choe Y, Kwon E, Rigon L G, Baek Y and Kim H Y 2024 *Soft Matter* **20** 2777
[20] Fares J, Fares M Y, Khachfe H H, Salhab H A and Fares Y 2020 *Signal Transduct. Target. Ther.* **5** 28
[21] Hiraki H L, Matera D L, Wang W Y, Prabhu E S, Zhang Z, Midekssa F, Argento A E, Buschhaus J M, Humphries B A, Luker G D, Pena-Francesch A and Baker B M 2023 *Acta Biomater.* **163** 378
[22] Mierke C T 2019 *Rep. Prog. Phys. Phys. Soc. G. B.* **82** 064602
[23] Wu J S, Sheng S R, Liang X H and Tang Y L 2017 *Future Oncol.* **13** 991
[24] Alberts B, Johnson A, Lewis J, Raff M, Roberts K and Walter P 2002 *Molecular Biology of the Cell* (4th edn.) (New York: Garland Science) pp. 18–249
[25] Singh A, Soler J A, Lauer J, Grill S W, Jahnel M, Zerial M and Thutupalli S 2023 *Nat. Phys.* **19** 1185
[26] Potiguar F Q, Farias G A and Ferreira W P 2014 *Phys. Rev. E* **90** 012307
[27] Shi S J, Li H S, Feng G Q, Tian W D and Chen K 2020 *Phys. Chem. Chem. Phys.* **22** 14052
[28] Qian B S, Tian W D and Chen K 2021 *Phys. Chem. Chem. Phys.* **23** 20388
[29] Kim W K, Chudoba R, Milster S, Roa R, Kanduč M and Dzubiella J 2020 *Soft Matter* **16** 8144
[30] Zhu W J, Huang X Q and Ai B Q 2018 *Chin. Phys. B* **27** 080504
[31] Kim Y, Joo S, Kim W K K and Jeon J H 2022 *Macromolecules* **55** 7136
[32] Cho H W, Kim H, Sung B J and Kim J S 2020 *Polymers* **12** 2067
[33] Lu Y and Hu G H 2021 *Soft Matter* **17** 6374
[34] Shan W J, Zhang F, Tian W D and Chen K 2019 *Soft Matter* **15** 4761
[35] Ning L H, Liu P, Ye F F, Yang M C and Chen K 2021 *Phys. Rev. E* **103** 022608
[36] Liu P, Ning L H, Zong Y W, Ye F F, Yang M C and Chen K 2022 *Phys. Rev. Lett.* **129** 018002
[37] Shaebani M R, Wysocki A, Winkler R G, Gompper G and Rieger H 2020 *Nat. Rev. Phys.* **2** 181

[38] Martí-Gómez A, Levis D, Díaz-Guilera A and Pagonabarraga I 2018 *Soft Matter* **14** 2610
[39] Tian W D, Gu Y, Guo Y K and Chen K 2017 *Chin. Phys. B* **26** 100502
[40] Zhou Y J, Wang T H, Lei X K and Peng X G 2024 *Chaos Solitons Fractals* **180** 114596
[41] Nagai K H, Sumino Y, Montagne R, Aranson I S and Chaté H 2015 *Phys. Rev. Lett.* **114** 168001
[42] Wang W 2023 *J. Am. Chem. Soc.* **145** 27185
[43] Hrishikesh B and Mani E 2023 *Soft Matter* **19** 225
[44] Ma Z, Lei Q L and Ni R 2017 *Soft Matter* **13** 8940
[45] Pan J X, Wei H, Qi M J, Wang H F, Zhang J J, Tian W D and Chen K 2020 *Soft Matter* **16** 5545
[46] Weeks J D, Chandler D and Andersen H C 1971 *J. Chem. Phys.* **55** 5422
[47] Di Leonardo R, Angelani L, Dell'Arciprete D, Ruocco G, Iebba V, Schippa S, Conte M P, Mecarini F, De Angelis F and Di Fabrizio E 2010 *Proc. Natl. Acad. Sci. USA* **107** 9541
[48] VERLET L 1968 *Phys. Rev.* **165** 201
[49] Du Y F, Jiang H J and Hou Z H 2019 *Soft Matter* **15** 2020
[50] Kumar P and Chakrabarti R 2023 *Phys. Chem. Chem. Phys.* **25** 1937